

Performance Characteristics of TreePM codes

J.S. Bagla, Suryadeep Ray

Harish-Chandra Research Institute, Chhatnag Road, Jhansi, Allahabad-211019

Abstract

We present a detailed analysis of the error budget for the TreePM method for doing cosmological N-Body simulations. It is shown that the choice of filter for splitting the inverse square force into short and long range components suggested in Bagla (2002) is close to optimum. We show that the error in the long range component of the force contributes very little to the total error in force. Errors introduced by the tree approximation for the short range force are different from those for the inverse square force, and these errors dominate the total error in force. We calculate the distribution function for error in force for clustered and unclustered particle distributions. This gives an idea of the error in realistic situations for different choices of parameters of the TreePM algorithm. We test the code by simulating a few power law models and checking for scale invariance.

Key words: gravitation, methods: numerical, cosmology: large scale structure of the universe

PACS: 95.75.-z, 98.65.-r

1 Introduction

Cosmological N-Body simulations have played a crucial role in improving our understanding of formation of large scale structure. These have filled large gaps in a domain where analytical solutions do not exist. N-Body simulations have also played a useful role by testing scaling relations derived from physically motivated ansatze.

Limitations of computing resources and our ability to simulate physical processes numerically have meant that N-Body simulations give only approximate solutions. It is possible to test whether the approximations in evolution of the

Email addresses: jasjeet@mri.ernet.in (J.S. Bagla), surya@mri.ernet.in (Suryadeep Ray).

system affects estimation of physical quantities of interest so the results are generally more reliable than those based on approximate evolution of the system.

A large number of methods have been used for doing Cosmological N-Body simulations (Bertschinger , 1998). All of these use some approximation for calculation of force. Approximations are used because direct summation over all pairs of particles scales as $O(N^2)$, where N is the number of particles, making the calculation very time consuming for large N . The use of these approximations reduces the number of calculations required to $O(N \ln N)$ or less. These approximations also introduce inaccuracies in the computed force.

The TreePM code (Bagla , 2002), that we study here, is a hybrid technique for carrying out large N-Body simulations to study formation and evolution of large scale structures in the universe. It is a combination of the Barnes and Hut (1986) Tree code and a Particle-Mesh code (Hockney and Eastwood , 1988). The TreePM method combines high resolution of tree codes with the ability of PM codes to compute the long range force with periodic boundary conditions.

In this paper we carry out a comprehensive study of the TreePM code. We analyse errors in estimation of force in both the tree and the PM components, and also study the distribution of errors for different distributions of particles. We also study the variation of CPU time required for the TreePM code as we vary parameters describing the mathematical model of this method.

2 TreePM method

A large number of methods have been suggested for improving the PM method by combining it with other methods of computing force at small separations (Efstathiou et al , 1985; Couchman , 1991; Xu , 1995) to reduce the softening length below the grid length cutoff imposed by the PM method. A common failing of nearly all such methods is that these continue to use the usual PM force, which is known to have large errors and anisotropies at scales comparable to the grid scale (Bouchet and Kandrup , 1985). These errors are present in the final force, and there is no natural way of reducing the errors in any of these methods.

The philosophy of TreePM method is to modify the PM force in order to have a better control over errors in the long range force. This is done by an explicit division of the potential and force into a long range and a short range component. PM method is then used to compute only the long range component, and the tree method is used to calculate the short range component. This can

be expressed in terms of equations as:

$$\varphi_{\mathbf{k}} = \varphi_{\mathbf{k}}^s + \varphi_{\mathbf{k}}^l \quad (1)$$

$$\varphi_{\mathbf{k}}^l = \varphi_{\mathbf{k}} F(kr_s, \dots) \quad (2)$$

$$\varphi_{\mathbf{k}}^s = \varphi_{\mathbf{k}} (1 - F(kr_s, \dots)) \quad (3)$$

Here, $\varphi_{\mathbf{k}}$ is the Fourier transform of the gravitational potential, $\varphi_{\mathbf{k}}^s$ and $\varphi_{\mathbf{k}}^l$ are the short range and the long range components, respectively. $F(kr_s, \dots)$ is a filter function that is unity for $kr_s \ll 1$ but decreases rapidly for $kr_s > 1$. Thus r_s is the scale at which the short range and long range forces are split. F can depend on other parameters apart from r_s .

This manner of splitting force permits us to control errors in both the components of force. What we require is a function $F(kr_s, \dots)$ that decreases sufficiently quickly at $kr_s > 1$. Similarly in real space, the short range potential and force should become negligible beyond a few r_s , and the long range force should be negligible below r_s . Bagla (2002) suggested $F = \exp[-k^2 r_s^2]$. This function has an added feature that it is positive definite, as is its Fourier transform. Relevant equations for this case are:

$$\varphi_{\mathbf{k}}^l = -\frac{4\pi G \rho_{\mathbf{k}}}{k^2} \exp[-k^2 r_s^2] \quad (4)$$

$$\varphi^l(r) = -\frac{Gm}{r} \operatorname{erf}\left(\frac{r}{2r_s}\right) \quad (5)$$

$$\varphi^s(r) = -\frac{Gm}{r} \operatorname{erfc}\left(\frac{r}{2r_s}\right) \quad (6)$$

$$\mathbf{f}^l(\mathbf{r}) = -\frac{Gm\mathbf{r}}{r^3} \left(\operatorname{erf}\left(\frac{r}{2r_s}\right) - \frac{r}{r_s\sqrt{\pi}} \exp\left(-\frac{r^2}{4r_s^2}\right) \right) \quad (7)$$

$$\mathbf{f}^s(\mathbf{r}) = -\frac{Gm\mathbf{r}}{r^3} \left(\operatorname{erfc}\left(\frac{r}{2r_s}\right) + \frac{r}{r_s\sqrt{\pi}} \exp\left(-\frac{r^2}{4r_s^2}\right) \right) \quad (8)$$

Here, erf is the error function and erfc is the complementary error function. Most of our study is restricted to the TreePM codes that use this filter.

We can generalise to more complex filter functions. We studied two families of functions:

$$F(kr_s, \alpha) = \exp\left[-\left(k^2 r_s^2\right)^{\alpha/2}\right] \quad (9)$$

$$F(kr_s, n) = \left(1 + k^2 r_s^2\right)^{-n} \quad (10)$$

Here α and n are additional parameters. For $\alpha = 2$ in eqn.(9), we recover the one parameter filter used in Bagla (2002). Fig.1 shows the ratios $|f^s/f^{tot}|$

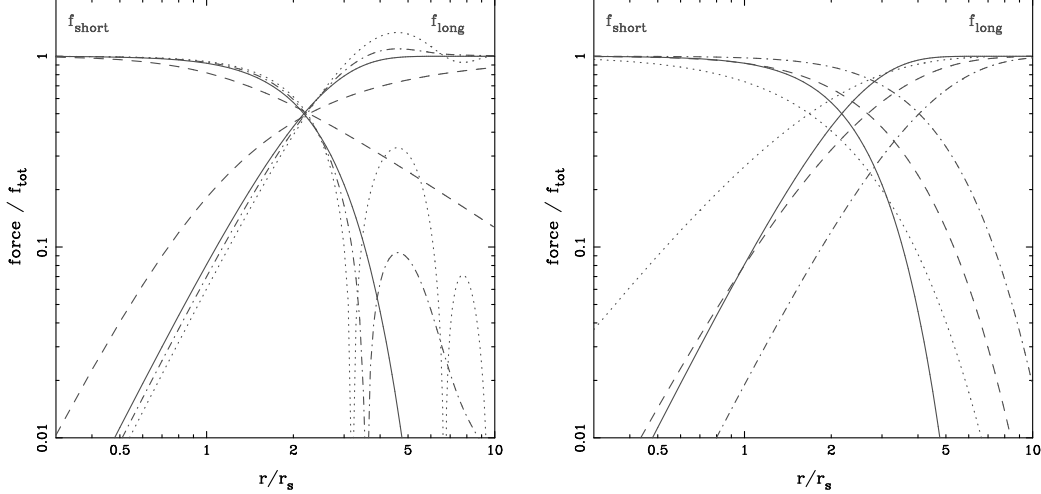


Fig. 1. We have shown the variation of the short range and the long range forces for a choice of filters in this figure. We have plotted the ratio of short-range/long-range force and the inverse square force as a function of distance scaled by the scale used for partitioning. Left panel shows curves for filters described by eqn.(9), and the right panel shows curves for filters described by eqn.(10). For reference, we have also plotted the curve corresponding to $\alpha = 2$ on the left panel. In the left panel, dashed curve, solid curve, dot-dashed curve and dotted curve correspond to $\alpha = 1.0, 2.0, 2.5$ and 4.0 respectively. In the right panel, the solid curve refers to $\alpha = 2.0$ and the dotted curve, dashed curve, and dot-dashed curve correspond to $n = 1, 2$ and 4 respectively.

and $|f^l/f^{tot}|$ as functions of scale r for these models. We have chosen $r_s = 1$ for this figure. Left panel shows these ratios for models described by eqn.(9) and the right panel shows models described by eqn.(10). In the left panel, we see that the short range force for $\alpha < 2$ decreases very slowly at large scales, making it an unsuitable choice. For $\alpha > 2$, the short range force oscillates at large scales and the amplitude of peaks decreases very slowly with scale. Hence these models too are not useful as an alternative to the $\alpha = 2$ model. Models described by eqn.(10) are shown in the right panel. In this case the behaviour is better than models with $\alpha \neq 2$ in that the long and the short range forces both fall off much faster. However, the model with $\alpha = 2$ is better than any of these models. This model is plotted in the right panel as the solid curve. We would like the overlap between the short and long range forces to be as small as possible. For one, a rapidly decreasing short range force implies that we need to sum this over a small region in space. Computation of the short range force is the most time consuming part and hence a sharply falling short range force is required for a well optimised code. The second reason which requires us to have a long range force that decreases rapidly below some scale is that the PM force typically has large errors at around grid scale. The main motivation of considering an explicit division of force in a long range and a short range component was to avoid carrying over the errors in the PM force by truncating the long range force at scales where PM contributes most

significantly to errors. Thus we want to use that filter for which the range of scales at which both the long range and the short range components are relevant is the smallest, and the Gaussian filter is the optimum one in this regard and no other filter comes close to this. We shall not discuss any other filter from this point onwards as figure 1 suggests that the Gaussian filter is the most optimum one.

3 Error Analysis

We shall first study errors in the force field of one particle. As the tree approximation does not have any errors for a single particle, we shall focus exclusively on errors in the long range force.

3.1 Errors in the Long Range Force

The long range force (eqn.(7)) is computed by the Particle-Mesh method. We summarise the PM method here, and for details we refer the reader to other sources (Hockney and Eastwood , 1988; Bouchet and Kandrup , 1985; Bagla and Padmanabhan , 1997). Particle positions are used to compute the density field on a regular mesh.¹ This is done using an interpolating function $W(x, x_i)$ that assigns mass of a particle at position x to mesh points x_i . In three dimensions, the interpolating function is a product of three one dimensional interpolating functions. Density field on the mesh is Fourier transformed using Fast Fourier transform (FFT). In Fourier space, we solve eqn.(4) instead of the usual Poisson equation. We multiply this with $i\mathbf{k}$ to get the negative gradient of the long range force in Fourier space. An inverse transform using FFT gives us the long range force on mesh points. This is interpolated back to particle positions using the same function W . In this scheme, mesh and the interpolating function W are the main sources of anisotropy. We use the cloud-in-cell (CIC) interpolating function (Hockney and Eastwood , 1988).

$$W(x, x_i) = 1 - |x - x_i|/L \quad |x - x_i| \leq L \quad (11)$$

$$= 0 \quad |x - x_i| > L \quad (12)$$

Here L is the separation between adjacent mesh points.

To estimate errors in the long range force, we follow the method described by Efstathiou et al (1985). We place a particle at a random position in a mesh cell and use our code to find the long range force. The force is evaluated

¹ We will use terms mesh and grid interchangeably in the context of PM codes.

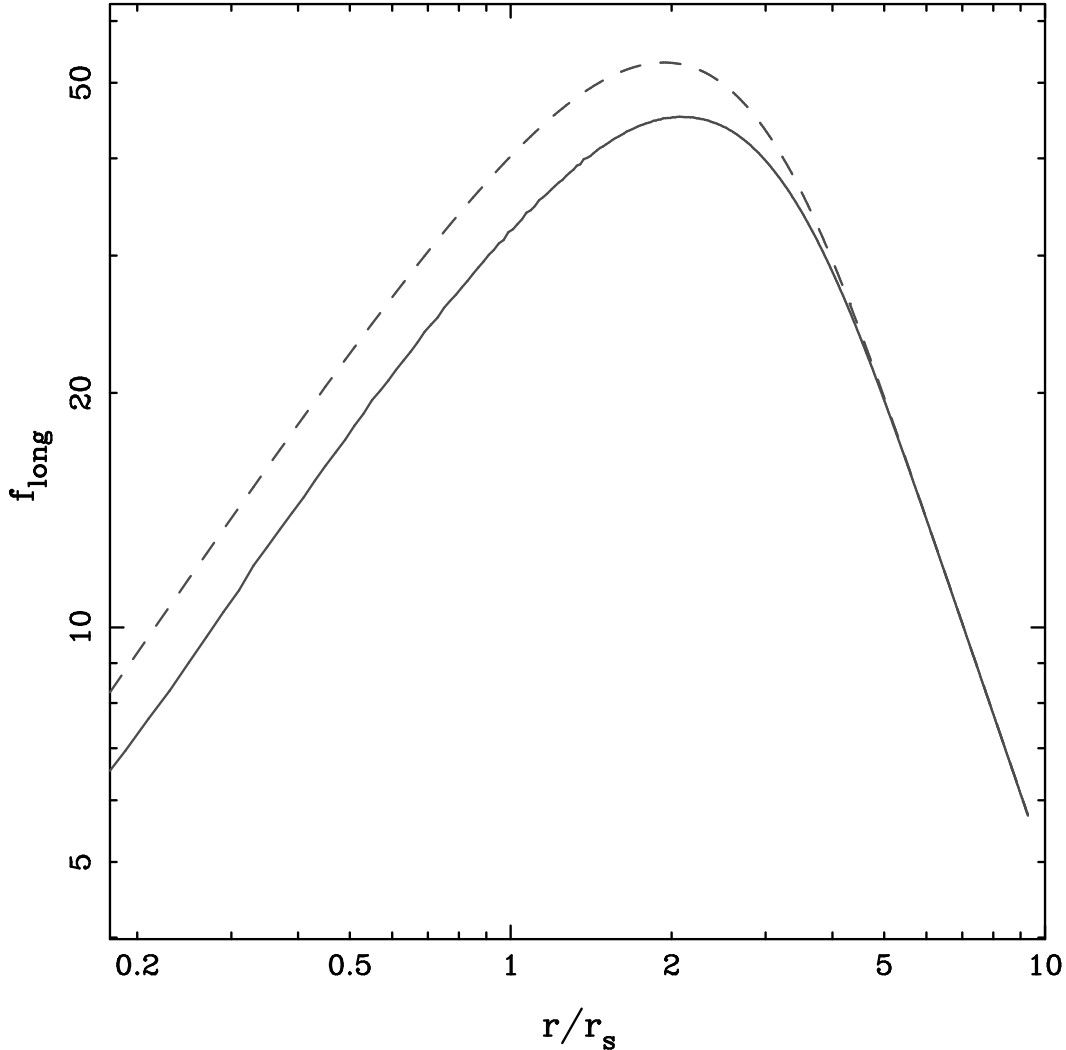


Fig. 2. Long range force for a single particle is shown as a function of distance. The dashed curve shows the expected long range force (eqn.(7)) and the thick curve shows the long range force obtained in the simulation. This curve was drawn for $r_s = L$. There is a clear under-estimation of the long range force at small scales. See text for details.

at a large number of random points scattered within some distance from the particle. This process is repeated a number of times with a different position of the particle. We use the force calculated this way to compute the average long range force as a function of distance as well as the dispersion about this average.

Figure 2 shows a plot of the average long range force (solid curve) and eqn.(7) (dashed curve) as functions of scale. This curve was drawn for $r_s = 1$. The average force clearly falls below the expected values at small scales.

This difference is caused mainly by the interpolating function. In the continuum limit we require the interpolating function to be like the Dirac delta

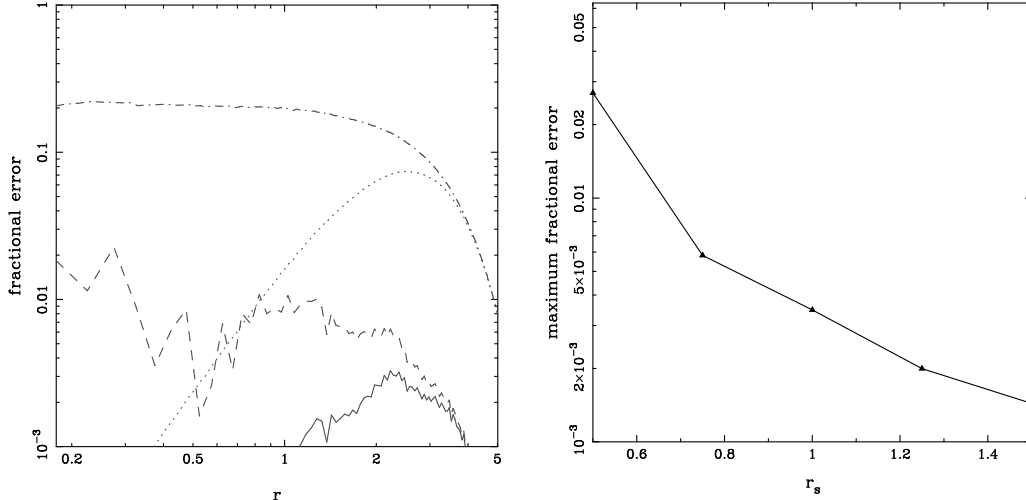


Fig. 3. Left panel shows the fractional error in the long range force due to a particle as a function of scale. Difference of the computed long-range force from eqn.(7) is scaled by the expected long range force for the dot-dashed curve. The same difference is scaled by the inverse square force and shown by the dotted curve. This latter curve is more relevant for studying the contribution to the error in force. Curves showing the fractional error after removing the effect of interpolating function are also shown here. Dashed curve shows the fractional error when scaled with the long range force and the solid curve shows the fractional error scaled with the inverse square force. See text for details of how the effect of interpolating function is removed. The peak fractional error when scaled by the inverse square force for this case is less than 0.4% for $r_s = L$. The right panel shows the peak fractional error as a function of r_s .

function. However, we cannot use that and hence there is a serious short-fall in the force at small scales. This becomes clear in Fourier space analysis (Bouchet and Kandrup , 1985; Hockney and Eastwood , 1988). Same analysis also suggests that by de-convolving the interpolating function, we should be able to recover the expected long range force. We deconvolve² the interpolating function twice, as we use it twice in force calculation: once for calculating the density on the mesh and then for calculating force at the positions of particles. For reference, we mention that the Fourier transform of the one dimensional CIC function is $4 \sin^2(kL/2)/(kL)^2$, where k is the wave number and L is the size of one mesh cell.

Such deconvolution of an arbitrary force will not work very well as it will only enhance anisotropies introduced by the mesh. However in this case contribution of wave modes near the Nyquist frequency is negligible due to the Gaussian filter. So we are essentially trying to correct for the amplitude at in-

² We divide the potential in k-space by the square of the Fourier transform of the interpolating function. Since the three dimensional interpolating function is product of the three one dimensional interpolating functions, we are essentially dividing φ_k by $W_{k_x}^2 W_{k_y}^2 W_{k_z}^2$. Square of each of these needs to be taken as we need to do the deconvolution two times.

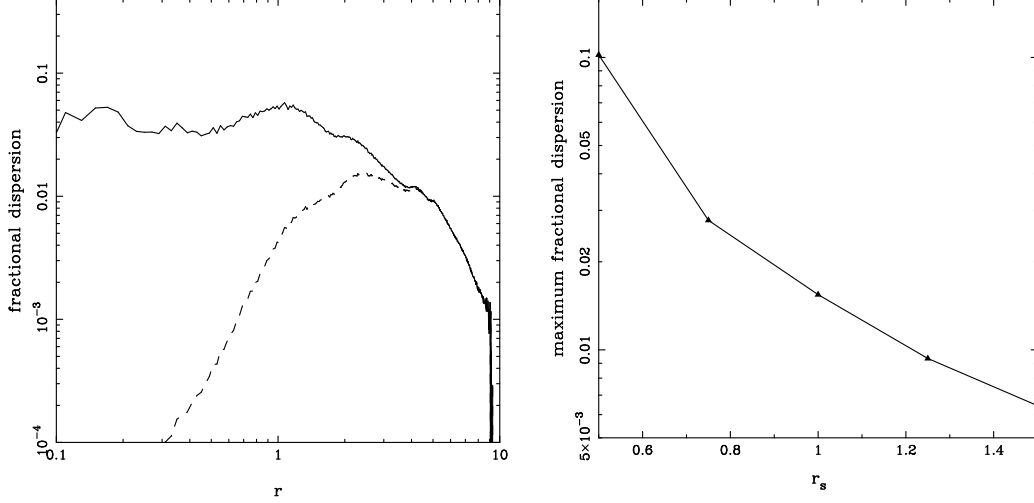


Fig. 4. Dispersion about the average long range force for $r_s = 1$ with deconvolution of the interpolating window function. This dispersion scaled by the long range force is shown by the solid curve. Dispersion scaled by the inverse square force is shown by the dashed line. The peak dispersion in this case is just over 1.4% of the inverse square force. The right panel shows the maximum value of dispersion scaled by the inverse square force as a function of r_s .

intermediate wave numbers. Partial correction can be obtained by de-convolving for the effect at small wave numbers by considering the Taylor expansion of W_k about $k = 0$ (White , 2000).

The effect of deconvolution on the long range force is shown in figure 3. We have plotted the difference of the average long range force and eqn.(7) divided by the long range force. We have also plotted the difference divided by the total force because it is this quantity that is relevant for errors in the total force. We have plotted these for the average force shown in figure 2 as well as the average force obtained after deconvolution described above. The effect of deconvolution is striking—the difference between the average long range force and eqn.(7) normalised by the total force drops by nearly one order of magnitude. Fractional error drops below 1% and is below 0.4% for the entire range of scales. One can lower this further by using a larger r_s , or use a lower r_s if larger errors are acceptable. Figure 3 also shows the maximum of the difference between the average long range force and eqn.(7) normalised by the inverse square force as a function of r_s . As expected, this decreases as we increase r_s . Thus we can choose r_s once we have fixed the error that is acceptable for our physical application. We will use long range force with deconvolution of the interpolating function W in the following discussion.

From deviations of the average force from eqn.(7), we now turn to the dispersion in force about this average. Both these quantities are calculated in narrow bins in distance r . Figure 4 shows the dispersion in the long range force. We have plotted *rms* dispersion about the average force as a function of r . We

have normalised the dispersion with the long range force (eqn.(7)), and the total force. The latter curve is relevant for total force. From this curve we can see that the rms dispersion about the average long range force reaches a peak of about 1.4% near $r = 2r_s$.

The dispersion, just like the deviation of the average long range force from the theoretical expectation eqn.(7), decreases as we increase r_s . Figure 4 shows the variation of the maximum of *rms* dispersion normalised by the inverse square force, as a function of r_s .

We can summarise our investigations of the errors in the long range force for a particle as follows: Maximum deviation of the long range force from the theoretical expectation is around 0.4% and this deviation is much smaller at most scales. Dispersion about the average peaks at a value of 1.4% and is well below 1% for most scales. These values are for $r_s = L$ and the maxima of errors occur around $2r_s$, errors fall off rapidly on both sides. Errors decrease as we increase r_s .

We will not study errors in the long range force for a system of particles. We will, instead, study the error in the total force after studying the errors in the short range force.

4 Errors in the Short Range Force

The short range force is calculated using the tree approximation. We use the Barnes and Hut (1986) method. In this method, the simulation volume is taken to be a cube. Particles are arranged in a hierarchy of cells in an oct-tree, i.e., each cell can have up to eight daughter entities. These can either be cells or particles. The simulation volume is divided into smaller cells so that at the smallest level, no cell contains more than one particle. Once the tree structure is set up, we calculate the position of the centre of mass for each cell as well as the total mass contained within it.

Tree approximation is then used to calculate force on each particle. In this approximation, distant cells are treated as point masses with all the mass concentrated at the centre of mass. Error in force introduced by this approximation is proportional to the square of the ratio of size of the cell (d) to the distance (r) to the centre of mass from the point where force is being calculated. We define this ratio as $\theta = d/r$. The error in force is proportional to θ^2 . In order to control errors, we would not like to use cells that are too close or too large. This is done by introducing a cell acceptance criterion, e.g. by

computing the quantity θ and comparing it with a threshold θ_c :

$$\theta = \frac{d}{r} \leq \theta_c \quad (13)$$

The error in force will obviously increase with θ_c . It can be shown that the maximum error for inverse square force is $9\theta_c^2/4$. For a detailed discussion of cell acceptance criteria and error in force, we refer the reader to several detailed studies (Hernquist , 1987; Salmon and Warren , 1994; Springel, Yoshida and White , 2001).

The tree approximation is used here for computing the short range force which differs from the usual inverse square force. We expect errors to be different in this case. We calculate the error at leading order in tree approximation and compare it with the corresponding error in the case of inverse square force.

We take a cubical cell of dimension d and distribute point masses randomly inside it. Our aim is to calculate the error involved in computing the short range force in the tree approximation on a unit point mass situated at the origin due to the masses in the cubical cell described above. To calculate the error, we need to compare the short range force in the tree approximation (\mathbf{f}_{cm}^s) with the sum of short range forces due to all the particles in this cell (\mathbf{f}^s). We also have the inverse square force in the tree approximation \mathbf{f}_{cm} .

To quantify error in short range force we define ϵ^s as a measure of the error in the computed short range force.

$$\epsilon_s = \frac{|\mathbf{f}_{cm}^s - \mathbf{f}^s|}{|\mathbf{f}_{cm}|} \quad (14)$$

We compute the error in case of the inverse square force for comparison. The worst case we can have is if two particles are at diagonally opposite ends of the cell, and the origin is along the same diagonal. The distance between the particles is $d\sqrt{3}$, and the fractional error in force upto leading order in θ_c is $9d^2/(4r^2) = 9\theta_c^2/4$ where r is the distance from the origin to the centre of mass. If the two particles are separated along an edge of the cell instead of the diagonal, the error is $3\theta_c^2/4$. A similar analysis for the short range force gives

$$\begin{aligned} \epsilon_s = & \frac{3\theta_c^2}{4} \left[\operatorname{erfc} \left(\frac{r}{2r_s} \right) + \left(\frac{r}{r_s} \right) \exp \left(-\frac{r^2}{4r_s^2} \right) \right] \\ & + \frac{\theta_c^2}{4} \left[\frac{2}{\sqrt{\pi}} \left(\frac{r}{r_s} \right)^3 \exp \left(-\frac{r^2}{4r_s^2} \right) + \frac{1}{8\sqrt{\pi}} \left(\frac{r}{r_s} \right)^5 \exp \left(-\frac{r^2}{4r_s^2} \right) \right]. \end{aligned} \quad (15)$$

Here we have also assumed that the separation between the two particles is smaller than r_s . Error here has been calculated for the case when the two

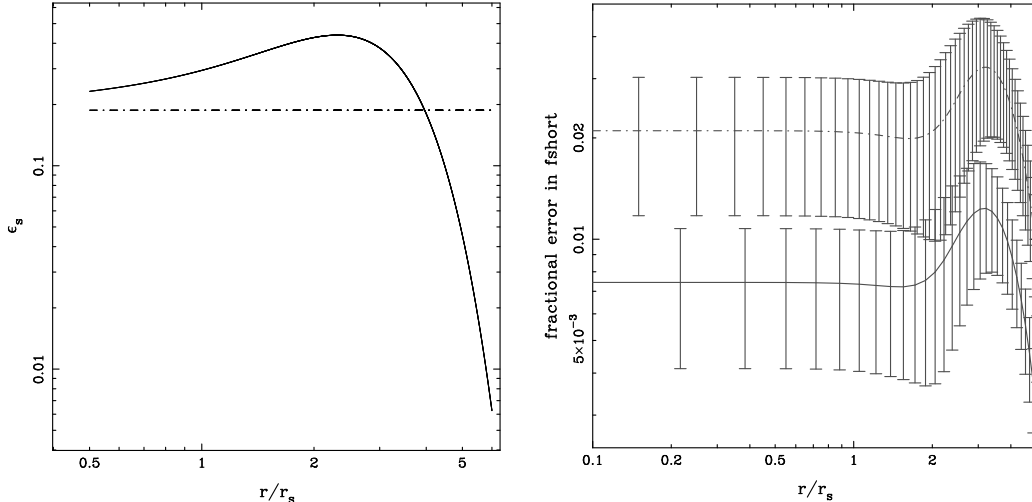


Fig. 5. Fractional error in the tree approximation in one of the worst cases is shown in the left panel as a function of distance r for the short range force (solid curve). This is the error up to leading order in θ_c (see text). For reference, we have also plotted the corresponding error in case of the inverse square force (dot-dashed curve). This error is computed for the case when the two particles are separated along an edge of the cell and the two particles and the point where force is being calculated are along a line. The right panel shows fractional error in short range force measured using the method described in text. Here, the solid curve corresponds to $\theta_c = 0.3$ and $N_p = 30$ and the dot-dashed curve is for $\theta_c = 0.5$ with the same number of particles. Error bars mark 1σ variation about the average error measured for 100 different distributions of particles.

particles are separated along an edge of the cell and the origin (where the force is being calculated) and these two points are collinear. We have plotted the error as a function of distance r in fig.5.

Now we turn to a more realistic estimate of error for random distribution of particles in the cell, instead of considering pathological situations which give rise to large error. Right panel of figure 5 shows the fractional error in short range force ϵ_s as a function of distance r . Error is constant at small scales, increases around the scales where the contribution of short range force is decreasing rapidly, then plummets to very small values at larger scales. The range of scales where the error is large are those where the short range force contributes a significant fraction to the total force *and its variation with distance is significantly different from inverse square*. In the figure, error is plotted for two values of θ_c . It is lower for smaller θ_c : error for $\theta_c = 0.3$ is a nearly a factor three smaller than for $\theta_c = 0.5$. Here error has been averaged over 100 different distributions of 30 particles in the cell. Error is smaller for larger number of particles as chances of an extreme distribution of particles become smaller. Even for $N_p = 10$, the error is considerably smaller than the extreme case we used for estimating errors above. Error for $\theta_c = 0.5$ and $N_p = 30$ is about 2%, slightly larger than the maximum error due to long

range force (1.4% for $r_s = L$). Errors for $\theta_c = 0.3$ are smaller and closer to the errors in the long range force. However, we should add that these are errors due to particles in a single cell. In a generic situation, these errors may cancel out or add up, depending upon the details of the particle distribution.

5 Errors in the TreePM force

We turn to the question of errors in the TreePM force calculated by adding the short range and the long range forces. Errors are calculated with respect to a reference force computed with the following configuration of the TreePM code. We chose $\theta_c = 0.01$, hence the errors in short range force are negligible as these errors decrease in proportion to θ_c^2 for the worst case scenario. We take $r_s = 4.0$ thus error in the long range force is below 0.2% if we extrapolate the maximum dispersion in long range force. With this setup, we can safely assume that the error in reference force (as compared to the inverse square force with periodic boundary conditions that we should use) is below 0.2% at all scales, and this is sufficient for studying errors in the TreePM force calculated using more pragmatic values of r_s and θ_c as we are aiming to keep errors below 1% level for most particles in all situations.

We will calculate errors for two very different distributions of particles, one a random distribution of particles with uniform density (unclustered distribution) and the other a clustered distribution generated by an N-Body simulation. We will present the results for these distributions side by side.

We present the results of our analysis by plotting the cumulative distribution for fractional error. Errors were calculated for a distribution of $2^{21} \simeq 2 \times 10^6$ particles so that we have sufficient number of particles to study the distribution.

We have presented the variation of errors with r_{cut} in fig. 6. For this figure we used $r_s = L$ and $\theta_c = 0.5$. r_{cut} is the radius within which we sum the short range force around each particle. We need to sum out to a distance where the contribution of the short range force to the inverse square force drops to an ignorable fraction. From fig. 1, we know that the short range force is less than 1% of the inverse square force at $5r_s$, so we expect that r_{cut} should be comparable to this value. We find that for the unclustered distribution, distribution of errors is very different for $r_{cut} = 3r_s$ as compared to $r_{cut} \geq 4r_s$. For all $r_{cut} \geq 4r_s$, distribution of errors is very similar. This can result if particles at scales beyond $4r_s$ are not contributing to the force. This is to be expected in a uniform distribution of particles. Distribution of errors for the clustered distribution is shown in the right panel of fig. 6. For the clustered distribution, the particle distribution is not homogeneous

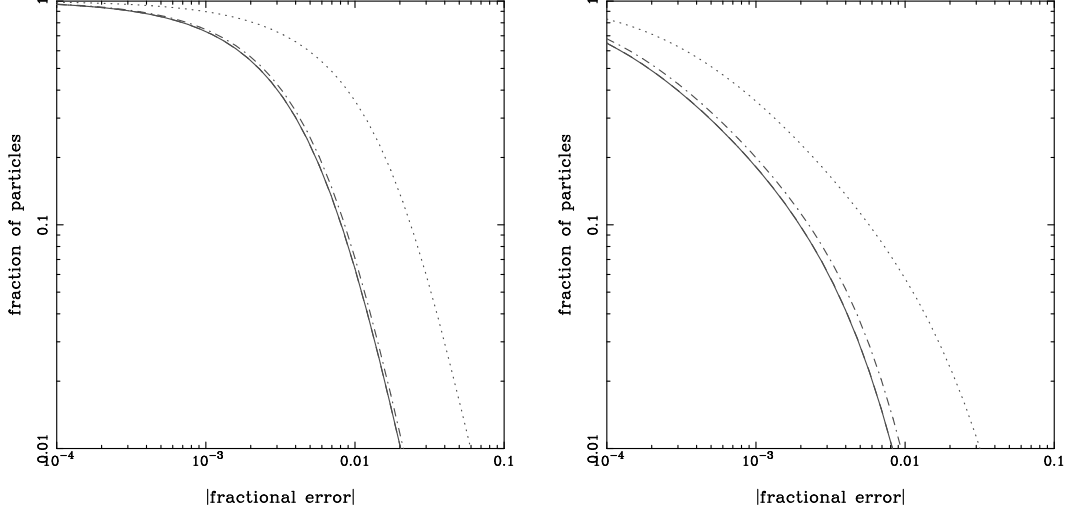


Fig. 6. The distribution of fractional error in the TreePM force is shown here for two distributions of particles. The left panel shows the distribution for a uniform distribution of particles, for different choices of r_{cut} , the radius within which the short range force is summed. The right panel shows the same for a clustered distribution of particles. We used $r_s = L$ and $\theta_c = 0.5$ for these figures. Solid curve corresponds to $r_{cut} = 6r_s$, dashed curve is for $r_{cut} = 5r_s$, dot-dashed and dotted curves correspond to $r_{cut} = 4r_s$ and $3r_s$ respectively. The error is very large in both cases for $r_{cut} = 3r_s$. The error for all $r_{cut} \geq 4r_s$ is essentially the same. There is some difference in the error for $r_{cut} = 4r_s$ and $r_{cut} \geq 5r_s$ for the clustered distribution, as anisotropies in the particle distribution start to make the force from particles at these distances more and more significant.

and hence particles at larger distances contribute significantly to the force on each particle. As this contribution increases, force from $r > 4r_s$ becomes more relevant. Error distribution for the clustered distribution shows small differences between $r_{cut} = 4r_s$ and $r_{cut} \geq 5r_s$. From these figures we conclude that $r_{cut} = 5r_s$ is a safe choice and that $r_{cut} = 4r_s$ will suffice for most purposes.

Figure 7 shows the distribution of errors for different values of θ_c . As before, we have shown results for the unclustered distribution in the left panel and that for the clustered distribution in the right panel. We used $r_s = L$ and $r_{cut} = 6r_s$ for these plots. There is a marked difference in errors for different values of θ_c in case of unclustered distribution. Error decreases with θ_c , the variation decreases as we get to smaller values of θ_c . Situation is somewhat different for the clustered distribution as there is hardly any difference between errors for different values of θ_c . This suggests that the errors are dominated by errors in the long range force for clustered distribution. For unclustered distribution, the total force on each particle is small, whereas force due to a cell with many particles is large and many large contributions cancel out to give a small net force. Numerical errors in adding and subtracting large numbers seem to dominate errors in case of the uniform distribution. Contribution of cells is large for larger θ_c , hence we get a significant variation with θ_c for unclustered

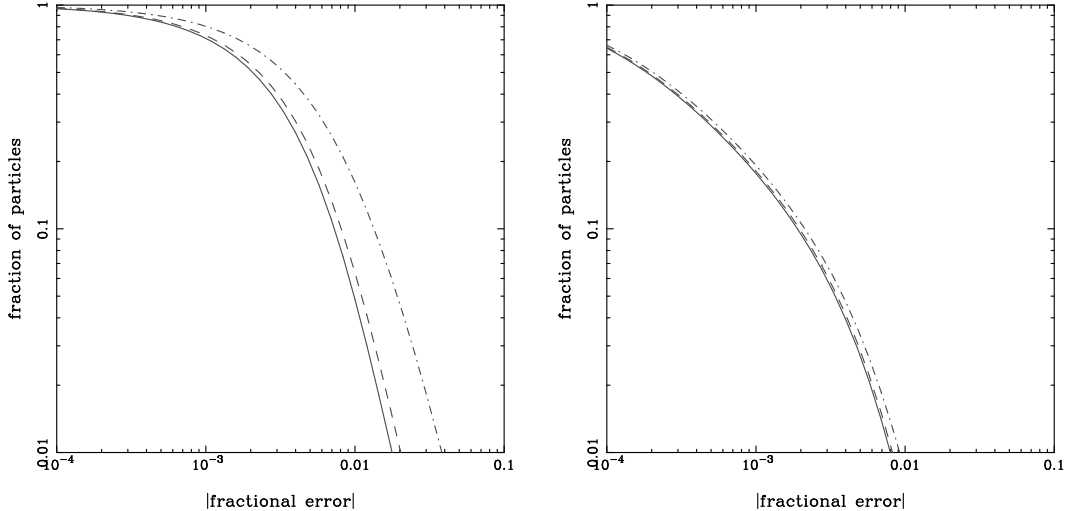


Fig. 7. The distribution of fractional error in TreePM force is shown here for different values of θ_c . The left panel shows these for a uniform distribution of particles and the right panel shows the same for a clustered distribution of particles. We used $r_s = L$ and $r_{cut} = 6r_s$ for these figures. Full line, dashed line and dot-dashed line correspond to $\theta_c = 0.3, 0.5$ and $\theta_c = 0.7$ respectively in both panels. The order of curves in both these cases is as expected, error is smaller for smaller θ_c . The difference in error with different θ_c reduces with increasing clustering. See text for an explanation.

distribution.

Lastly, we look at variation of errors with r_s . Figure 8 shows the distribution of errors for different values of r_s . We fixed the values of other parameters to $r_{cut} = 6r_s$ and $\theta_c = 0.5$. Left panel is for the unclustered distribution and the right panel is for clustered distribution of particles.

Errors for the clustered distribution increase monotonically as r_s is decreased. This is to be expected from our analysis of errors in the long range force. The fractional error in the TreePM force for 99% of the particles for $r_s = L$ is less than 0.8%. Variation of errors with r_s for the unclustered distribution is not monotonic. Errors decrease till r_s increases to unity, and then increase again. This happens because the small force on each particle for a uniform distribution again comes into play. For larger r_s , the force due to individual cells is large and numerical error in adding all the large contributions to get the small net force is also large. The fractional error in the TreePM force for 99% of the particles for $r_s = L$ is less than 1.5%, thus the variation in error from unclustered to clustered situation is small compared to that in tree codes. From this figure, we conclude that $r_s = L$ is the optimum choice for the TreePM code.

We can summarise the results of this study of errors as follows: Errors for 99% of particles are below 1.5% for unclustered distribution and below 0.8% for

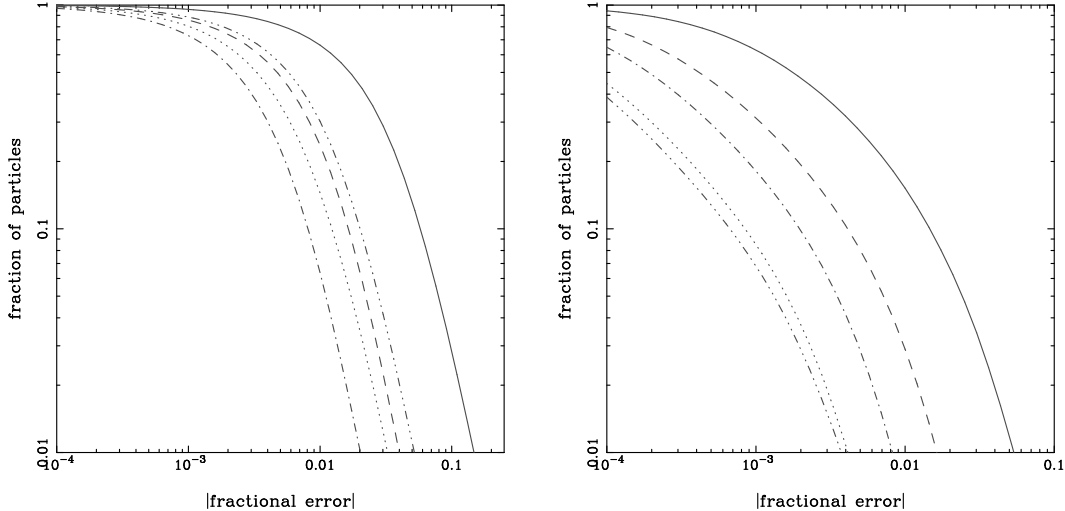


Fig. 8. Variation of error with r_s . The left panel shows the fractional error in TreePM force for a uniform distribution of particles and the right panel shows the same for a clustered distribution of particles. We used $\theta_c = 0.5$ and $r_{cut} = 6r_s$ for these figures. Different line styles are used for different values of r_s . Solid curve is for $r_s = 0.5L$, dashed curve for $r_s = 0.75L$, dot-dashed curve for $r_s = L$, dotted curve for $r_s = 1.5L$ and dot-dot-dashed curve is for $r_s = 2L$. The error decreases monotonically with increasing r_s for the clustered distribution. The behaviour is different for the unclustered distribution where the error decreases at first but then increases again. See text for an explanation.

clustered distribution for $r_s = L$, $r_{cut} \geq 5r_s$ and $\theta_c \leq 0.5$. The best way to reduce errors is to use a larger r_s as varying the other two parameters leads to large differences between the clustered and the unclustered cases.

6 CPU time requirements

In this section we will list the CPU time required for one time step of the TreePM code for a simulation of 2^{11} particles. We will also study variation of this as we vary the parameters of the TreePM method.

The computer on which these timings were obtained is powered by a 1.6GHz Pentium 4 CPU. Programs were compiled using the Intel Fortran compiler (version 5.0) and double precision numbers were used throughout. Programs are written in Fortran 90/95.

The recommended configuration of the TreePM code uses $r_s = L$, $\theta_c = 0.5$ and $r_{cut} = 5r_s$. In this case one time step takes 740 seconds. Times taken for building the tree, calculating the long range force, calculating the short range force and moving particles are, for one time step, equal to 6.38 seconds, 26.70 seconds, 711.51 seconds and 0.25 seconds respectively. This implies that the

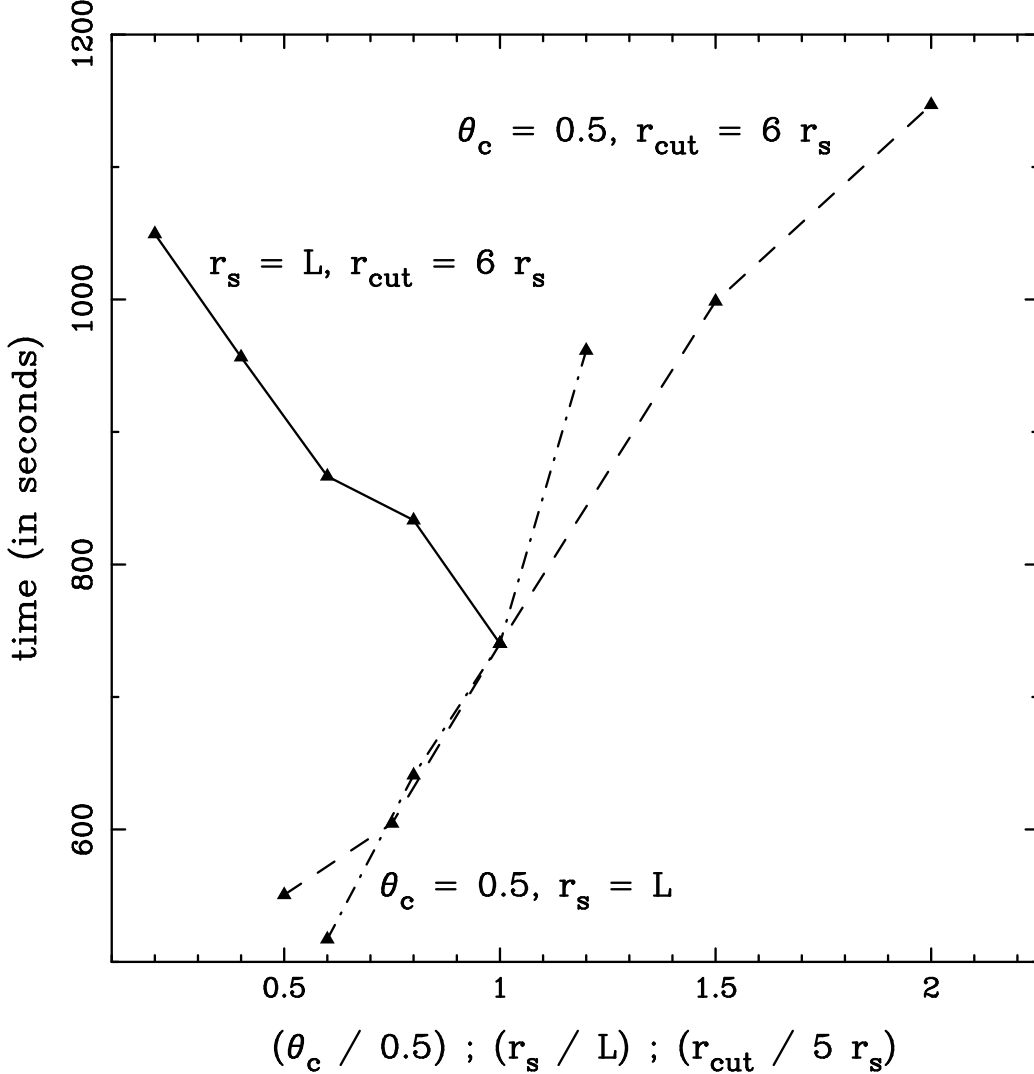


Fig. 9. Variation of CPU time required per time step is shown here as a function of changing parameters. The thick line shows the variation in CPU time with $\theta_c/0.5$. Points, from left to right, along this curve are for $\theta_c = 0.1, 0.2, 0.3, 0.4$ and 0.5 . Values of the other parameters were fixed to $r_s = L$ and $r_{cut} = 6r_s$. The dashed line shows the variation with respect to r_s/L at $r_{cut} = 6r_s$ and $\theta_c = 0.5$. The dot-dashed line shows the variation with $r_{cut}/5r_s$ with $\theta_c = 0.5$ and $r_s = L$.

time taken for each particle per step is 0.35ms. The quoted numbers are for an unclustered uniform distribution of 128^3 particles.

Time required for one time step of the TreePM code varies with the choice of parameters r_{cut} , r_s and θ_c . We expect the time taken to increase with increasing r_s and r_{cut} , and decrease with increasing θ_c . The behaviour for these cases is shown in fig. 9. It is seen that the time taken falls sharply with increasing θ_c , whereas errors are insensitive to the choice as long as $\theta_c \leq 0.5$. Therefore it makes sense to use $\theta_c = 0.5$. Time taken rises sharply with increasing r_{cut} . Again, by comparing with the variation of errors, we recommend $r_{cut} \approx 4.5r_s$.

Lastly, time taken increases rapidly as we increase r_s . We recommend $r_s = L$ as the error is minimum for this choice for the unclustered distribution.

7 Integrating the equation of motion

Our discussion so far has dealt only with evaluation of force. This is the main focus of this paper as the key difference between the TreePM and other methods is in the scheme used for evaluation of force. However for the sake of completeness, we give here details of integration of equations of motion. The usual form of the equation of motion is:

$$\begin{aligned} \ddot{\mathbf{x}} + 2\frac{\dot{a}}{a}\dot{\mathbf{x}} &= -\frac{1}{a^2}\nabla\phi \\ \nabla^2\phi &= 4\pi G a^2(\rho - \bar{\rho}) \end{aligned} \quad (16)$$

Here \mathbf{x} is the comoving coordinate, a is the scale factor, ρ is the density and $\bar{\rho}$ is the average density of the universe. Dot represents differentiation with respect to time. We can recast these equations in the following form:

$$\begin{aligned} \mathbf{x}'' + \frac{2}{a} \left\{ 1 + \left(\frac{1}{4} \right) \frac{2\Omega_\Lambda a^3 - \Omega_0}{\Omega_\Lambda a^3 + \Omega_0 + a(1 - \Omega_0 - \Omega_\Lambda)} \right\} \mathbf{x}' \\ = - \left(\frac{3\Omega_0}{2a^2} \right) \frac{1}{\Omega_\Lambda a^3 + \Omega_0 + a(1 - \Omega_0 - \Omega_\Lambda)} \nabla\psi \\ \nabla^2\psi = \delta = \frac{\rho}{\bar{\rho}} - 1 \end{aligned} \quad (17)$$

Here prime denotes differentiation with respect to the scale factor. Ω_0 is the density parameter of non-relativistic matter, Ω_Λ is the density parameter of the Cosmological constant and δ is the density contrast. We use a modified gravitational potential ψ . The equation of motion contains a velocity dependent term and hence we cannot use the usual leap-frog method. We recast the leap-frog method so that velocities and positions are defined at the same instant (Hut, Makino and McMillan, 1995). We solve the equation for velocity iteratively. Time step is chosen to be a small fraction of the smallest dynamical time in the system at any given stage. The fraction to be chosen is fixed by doing some tests.

One of the tests we did was to check for scale invariance in evolution of power law spectra. A simulation is repeated with different choices of time step until we find the largest time step for which we can reach the highly non-linear regime ($\bar{\xi} > 100$) and retain scale invariance. We then use a time step that is half of this largest time step. Figure 10 shows $\bar{\xi}$ as a function of $r/r_{nl}(t)$

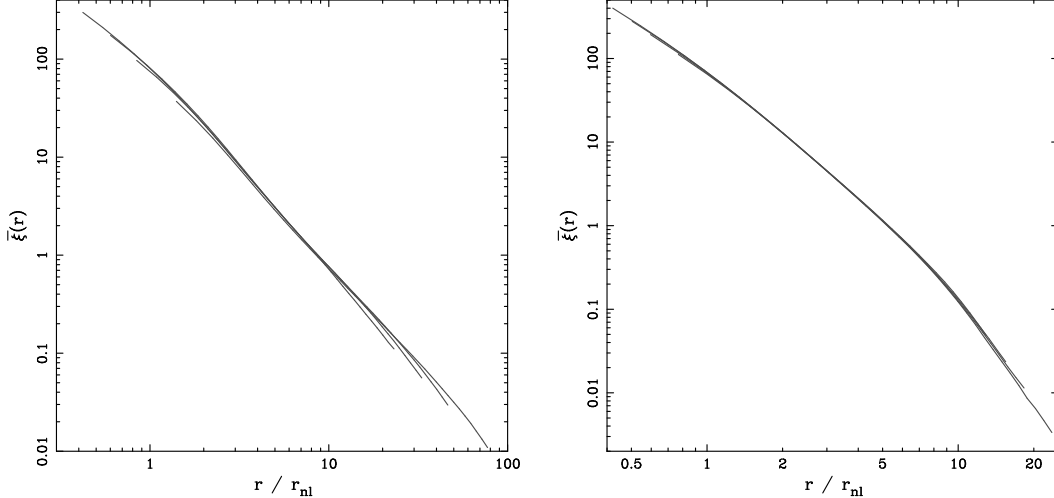


Fig. 10. This figure shows $\bar{\xi}$ as a function of $r/r_{nl}(t)$ for several epochs. Here $r_{nl}(t)$ is the scale which is going non-linear at time t and it varies in proportion with $a^{2/(n+3)}$ in the Einstein-deSitter model. n is the index of the power spectrum, we have used $n = -1$ for the left panel and $n = 1$ for the right panel. We have only plotted $\bar{\xi}$ at scales more than four times larger than the artificial softening length used in the simulation.

for several epochs. Here $r_{nl}(t)$ is the scale which is going non-linear at time t and it varies in proportion with $a^{2/(n+3)}$ in the Einstein-deSitter model. n is the index of the power spectrum. We have used $n = -1$ for the left panel and $n = 1$ for the right panel. We have only plotted $\bar{\xi}$ at scales more than four times larger than the artificial softening length used in the simulation. Scale invariance holds for both the spectra and we are able to probe the highly non-linear regime with this code.

8 Discussion

In this paper we have presented a detailed study of performance characteristics of the TreePM method. We have analysed different sources of error and suggested remedies for the main source of errors. The analysis of errors in realistic situations shows that the TreePM method performs very well and gives acceptably small errors.

This method compares favourably with other comparable methods such as implementations of the tree code like GADGET (Springel, Yoshida and White , 2001) and hybrid methods such as the TPM (Xu , 1995; Bode, Ostriker and Xu , 2002). From the numbers available in these papers, we find that the errors in the recommended configuration of the TreePM method are comparable with those in GADGET and lower than those in the TPM method. In terms of CPU time taken per step per particle, we again find that the numbers are

comparable. Of course, it is not possible to make a detailed comparison of this quantity as the whole approach is different. E.g., we do not use multiple time steps whereas GADGET relies heavily on these to optimise the speed. On the other hand GADGET and TreePM have a uniform force resolution whereas TPM does not and hence the time taken is likely to vary more strongly with the amplitude of clustering for the TPM code as compared to the other two.

Splitting of force into a short range and a long range part has a useful implication in terms of parallel implementation. Unlike the tree methods, the TreePM method involves a considerably smaller overhead in terms of inter-process communication and hence is likely to score over other methods in terms of scaling for a very large number of CPUs. In summary we can state that TreePM is a competitive method for doing Cosmological N-Body simulations. Explicit use of three parameters gives users control over errors and CPU time required.

Acknowledgements

A part of the work reported here was done using the Beowulf at the Harish-Chandra Research Institute (<http://cluster.mri.ernet.in>).

References

- Bagla J.S. and Padmanabhan T. 1997, *Pramana – Journal of Physics* 49, 161
Bagla J.S. 2002, *Journal of Astrophysics and Astronomy*, in Press.
Bagla J.S. 2002, Preprint. To appear in proceedings of the *Numerical Simulations in Astrophysics*, Tokyo, July 2002.
Barnes J. and Hut P. 1986, *Nature* 324, 446
Bertschinger E. 1998, *ARA&A* 36, 599
Bouchet F.R. and Kandrup H.E. 1985, *ApJ* 299, 1
Bode P., Ostriker J. and Xu G. 2000, *ApJS* 128, 561
Couchman H.M.P. 1991, *ApJL* 368, L23
Efsthathiou G., Davis M., Frenk C.S. and White S.D.M. 1985, *ApJS* 57, 241
Hernquist L. 1987, *ApJS* 64, 715
Hockney R.W. and Eastwood J.W. 1988, *Computer Simulation using Particles*, (New York: McGraw Hill)
Hut P., Makino J. and McMillan S. 1995, *ApJL* 443, 93
Salmon J.K. and Warren M.S. 1994, *J.Comp.Phys.* 111, 136
Springel V., Yoshida N. and White S.D.M. 2001, *New Astronomy* 6, 79
White M. 2000, Private communication.
Xu G. 1995, *ApJS* 98, 355